Magrathea: Magnificent Analysis of Grains Research At Tremendously High and Exciting Altitude

Dust growth experiment in micro-gravity conditions

Adrián Banos García, Adrián Castanón Esteban, Fabio Fabozzi, Marta Goli, Jonas Greif, André Guerra, Lisa Jonsson, Victoria Lofstad, Marine Martin-Lagarde, John McClean, Mattia Reganaz, Julia Seibezeder, Esmee Stoop, Gwenaël Van Looveren, Jophiel Wiis, Anton Ivanov, and Kieran Leschinski

(Alpbach Summer School 2017)

July 26, 2017

ABSTRACT

One of the the least understood processes in astrophysics is the formation of planetesimals from molecules and dust in the protoplanetary disks. In this paper we propose a mission to study the very first stages of planet formation, where small dust aggregates collide in the protoplanetary disk and grow into bigger clusters. During the mission, 28 experiments will be performed using different dust compositions, sizes and shapes in order to better understand under which conditions dust grains stick and aggregate. Each experiment will last for up to one month, with relative collision velocities of up to $5\,\mathrm{mms}^{-1}$ and initial dust sizes between $1\,\mu\mathrm{m}$ and $100\,\mu\mathrm{m}$. The experiment volume is approximately $6\,\mathrm{m}^3$, and at least 10^6 collisions per experiment will provide statistically significant results. The experiment will be launched on a Soyuz into a Sun-synchronous orbit at an altitude of $800\,\mathrm{km}$. We describe details of the payload and satellite platform. The project cost is compatible with a Cosmic Vision M-class mission.

Key words. Dust, Space-Laboratory, Grain growth, Protoplanetary disc, Microgravity

1. Scientific Background

1.1. Grain Growth

Recent observations of exoplanetary systems [9, 13, 23] have revealed a wide variety of planets in the universe. While the processes involved in forming planets from planetesimals are relatively well researched, the processes involved in moving from dust particles to planetesimals are poorly understood. Shedding light on these processes is key to advancing our knowledge in the field of planetary formation. More specifically, by understanding the details of grain growth during planet formation, we will be able to gain insights into how our own Earth was formed.

Current state-of-the art research suggests that growth of particles mainly happens in the mid-plane of the protoplanetary disks, since the concentration of solid masses in this region is expected to be the highest [33]. Brownian motion of micron-sized particles causes slow collisions between the particles, and grains start to grow [8]. In this phase, the gas is still coupled to the dust and follows the Epstein regime.

The interaction between particles can involve different processes, such as sticking (Van Der Waals forces), mass transfer and fragmentation and they are very poorly understood at the moment. All Earth-based experiments must cancel out Earth gravity. This is possible by using drop towers [26] (≈ 5 seconds) or with parabolic flights [7] (20 seconds duration). Ground-based and space telescopes are only able to observe static distributions of particle size. We are not able to follow different physical processes influencing the formation of large grains and planetesimals. A number of numerical models already exists (e.g. Ref. [36]) to simulate growth of the grains. Laboratory studies have attempted to reproduce these interactions, how-

ever the experiments were restricted to small durations and limited sizes of the grains. These studies mainly used silicates for their experiments (e.g Ref. [7]).

However, it is hard to reproduce the environments found in protoplanetary disks, which result in a lot of unknown parameters that still need to be explored. Furthermore, the theories and simulations surrounding grain growth of dust particles from micron to kilometre sized objects contain a lot of gaps and are inconsistent with results from observations from space. It is therefore important to explore these unknown quantities to explain how dust particles grow into planetasimals.

To fill these gaps we must look into very small velocities in the $< \mathrm{mms}^{-1}$ range. The goal of this project is to understand the physics of dust growth at low relative velocities ($\Delta v < 5\,\mathrm{mm\,s}^{-1}$) in protoplanetary disks by observing the behaviour of dust grains in micro-gravity ($<10^{-6}$ g) over long time scales of several weeks. Parabolic flights only provide micro-gravity for time scales in the order of 10 seconds and also limit the volume and temperature conditions which are necessary to reproduce the environments in protoplanetary discs. To look into the evolution of these particles as a whole, as opposed to singular one-on-one collisions, more time is needed to observe grain growth. Furthermore Earth-based experiments are unable to precisely control the range of particle velocities. Hence parabolic flights are unsuitable for extended observations of grain growth.

The International Space Station (ISS) has also been used for several experiments to observe dust growth (details in the next section and in [10, 24]). Movement of the astronauts in the spacecraft caused significant disturbance to the micro-gravity conditions. Furthermore the ISS has a large number of uncontrolled electric and magnetic field. These effects combined

also discount the ISS from conducting experiments with sub-millimeter per second relative velocities in the dust.

A satellite mission will provide a continuous undistributed microgravity environment as well as the long time scales (10^6 second) needed to observe the growth of dust grains from the micro- to the milli-meter sizes By putting a space laboratory in orbit around Earth we will be one step closer towards answering the question "where do planets come from?".

1.2. Previous Experiments & Missions

Several previous experiments have been conducted to recreate dust aggregation in interplanetary disks [7, 11, 18]. Different properties of the dust grains have been varied to determine the criteria that lead to dust growth. The experiments mentioned above have studied collisions of equal-sized particles as well as particles with different masses and compositions [7]. Fig. 1 provides an overview of preceding experiments on dust growth, with small porous grains colliding. The dotted boxes shows experiments of different relative velocities between the colliding particles (x-axis) and the corresponding masses (y-axis). The coloured areas represent relative number of collisions expected by the model. We see the majority of collisions do not result in grain growth. Grain growth primarily in the "hit and stick"-regime in the lower left corner of the image. It is this previously not studied parameter space that we will investigate with the Magrathea mission.
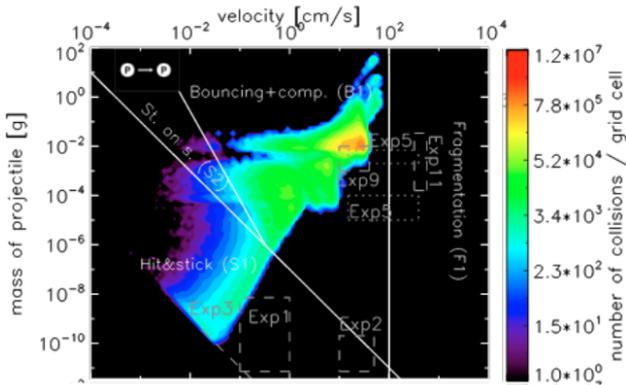

Fig. 1. Range of collision experiments performed (represented by the colour boxes) with the size (axes) and velocity in cm/s (background plot) between two non-fractal dust agglomerates (schematic taken from Ref. [18]).

Several test environments have been used to conduct experiments. Drop tower facilities can provide a microgravity environment for up to 5.18 seconds [26]. Several dust growth experiments have been conducted in drop towers [4, 5], but due to the short time range primarily two-particle systems have been studied. Other possibilities for performing microgravity experiments include parabolic flights and sounding rockets, providing 20 to 60 seconds respectively of continuous micro-gravity conditions. The Suborbital Particle Aggregation and Collision Experiment (SPACE) on board the suborbital rocket flight REXUS 12 studied the collision behaviour of submillimeter-sized dust aggregates [12]. Another sounding rocket experiment named The Cosmic Dust Aggregation (CODAG) aimed to investigate the Brownian motion-driven aggregation of cosmic dust [25].

Two dust aggregation experiments have been conducted on the ISS. It was found that angular submillimeter particles rapidly

formed clusters strong enough to survive turbulence in a proto-planetary nebula. Smaller particles generally aggregated more strongly and quickly than larger ones, while there was no strong dependence on composition. Round, smooth particles aggregated weakly or not at all [10, 24]. Even though the ISS can facilitate long duration experiments, the dust containers had to be shaken every 60 seconds to remove particles that stuck to the walls. One of the advantages of the Magrathea experiment is that it is not restricted to available space at the ISS. It will hence be able to have a much larger container that allows for longer time scales of the evolution of the dust cloud. This will provide the opportunity to observe the full range of grain growth over three orders of magnitudes in radius (from µm- to mm-scales).

As an extension of the ISS experiments, the CubeSat Q-PACE is under development to explore the fundamental properties of low-velocity (Δv <10 cm s^{-1}) particle collisions. The satellite will launch in December 2017 and is anticipated to run for three years. These two last experiments, the ISS and CubeSat experiment, were considered as the base for our developments. We intend to go one step further, by performing the experiments in a larger chamber and for a longer periods of time. We believe this will bring us one step closer to understanding the formation of planets.

2. Scientific Objectives

As stated above the knowledge of grain growth of µm-sized grains is not fully understood. Especially for particles with sizes of r_{eff} =30 µm to 100 µm at low relative incident velocities of Δv =0.001 mm s^{-1} to 1 mm s^{-1}, where r_{eff} is an equivalent radius of a sphere with the volume of the particle or grain. In order to observe grain growth, the size change of the colliding particles must be measured depending on several boundary conditions such as incident sizes of both colliding particles $r_{eff,1}$ and $r_{eff,2}$, relative incident velocities Δv, initial size distribution $n(r_{eff})$ (as an input parameter) and incident rotation frequency ν_{rot}.

How does the size of particles evolve with time, and how does size affect the outcome of collisions? We plan to condict experiments with mono-dispersed and poly-dispersed initial grain size distributions. The size of a grain is defined by the effective radius r_{eff}. As general initial particle size-distribution we will use $n(r_{eff}) \propto (\frac{r_{eff}}{0.005\,\mu m})^{-3.5}$ [30]. For the poly-dispersed size distributions we will use a size range of 0.1 µm to 100 µm and a size range of 20 µm to 30 µm as a wide and a narrow initial poly-dispersed size-distribution. For the mono-dispersed we will use initial size distributions of $\delta(r_{eff} - r_{eff,i})$ for $r_{eff,i} \in \{1\,\mu m, 30\,\mu m, 50\,\mu m, 100\,\mu m\}$.

Does grain shape influence grain growth? To second order approximations of the shape of dust are as a continuous distribution of randomly oriented ellipsoids (CDE). We believe that this approximation is not realistic to expect in nature. Therefore we suggest a random distribution of shapes for the initial shape distribution.

How does velocity affect grain growth? This requires measurements of velocities before collision, as well as size before and after. Measurements should be made in three axes and shall provide structure analysis of 10 µm grains.

How does rotation of the colliding particles affect grain growth? The relative velocity between the particles depends not only on the translational velocity, but on the rotational velocity as well. To study the effect of the rotation of the colliding

particles, the angular frequency, relative axis of rotation and precession will need to be determined. The frequencies of interest are in the interval between zero and 60 revolutions per second. If a cluster of dust of the size of 5 μm rotates with more than 40 revolutions per second, the centripetal forces exceed the Van Der Waals binding forces between the dust grains, and we would expect fragmentation of the cluster. If we however observe the cluster with a higher frequency, we know that there are more forces binding the particles together.

How does composition influence the grain growth? We want to measure how the composition of these different particles influence the collision results. The different compositions we are studying are SiO_2, with a density of $\varrho_{Si} = 2.2 \, \text{g cm}^{-3}$ [19], Fayalite (Fe_2SiO_4) with a density of $\varrho_{Fa} = 4.4 \, \text{g cm}^{-3}$, and the two mentioned compositions with an ice coating. It is known that silicates are observed in various parts of protoplanetary disk. However, the location and physical state of iron in protoplanetary disks still have to be confirmed. Iron is not observed in the gasses surrounding a young star and thus, it is expected to find it in the dust particles in the disk as mentioned in Ref. [22]. Furthermore, the impact of ice on the resulting interaction has not been studied in extend. Various studies show that the stickiness of ice can have a positive effect on the possibility of mass transfer and sticking particles [14, 34, 35]. To obtain the influence of these particles, a measurement of the change in size as a function of the composition of colliding grains is required.

How do temperature changes influence cohesion in icy agglomerates ? Several of the experiments will include dust particles coated in ice. The dust particles will be heated to 300 K for one hour to sublimate the ice. We want to measure if the agglomerates will fragment when the ice sublimates or stay together. This requires size measurements before and after heating of the particles. The experiment imitates agglomerates in a protoplanetary disc that move toward the star which cause the temperature to rise.

How does porosity affects grain growth and how do collisions of particles change the porosity? The porosity of the particle effect how easy a dust grain fragmentates or will be able to absorb the energy of the collision. We expect porose particle to stick together easier than for compact particles. We want to measure how the porosity effects the output interactions between particles. By implementing particles with different porosity distributions with a filling factor, $\phi \in [0.15, 0.65]$. This requires the tracking of the particles and the measurement of the porosity before and after the interaction of both particles. Obtaining the distributions of porosity among the particles before and after the experiments could be an alternative solution estimating the affects of porosity.

What are the collisional products? The outcome of a particle collision can be different variations of sticking (S), bouncing (B) and fragmentation (F). As categorised in Ref. [18] we are going to categorise particle collision into nine different kinds of collision outcome, as shown in Fig. 2. We will adapt this classification to facilitate for comparisons between out experiments and previous results. By recording the collisions, the outcome can be classified into different variations of sticking, bouncing and fragmentation.

An overview of the different types of experiments can be found in Table 2. In Table 1 a detailed overview of the scientific requirements can be found. To maintain a stable environment and acquire good statistics the experiment needs to meet several properties.
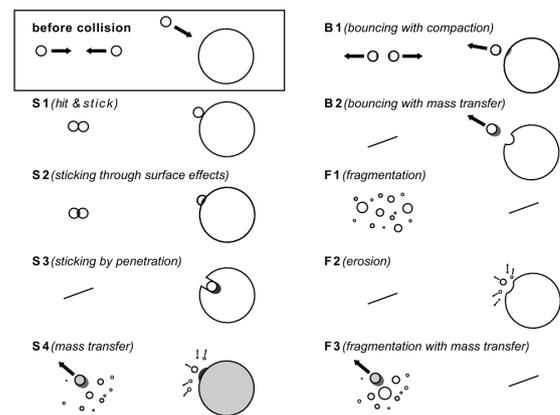

Fig. 2. Classification of different collision outcomes between two small particles, as well as and one small colliding with one large. The outcomes are various versions of sticking (S), bouncing (B) and fragmentation (F). (Figure taken from Ref. [17]).

Firstly, the volume must be big enough to ensure that the time of interaction between particles is much shorter than the time it takes for the particles to interact. This is realised by obtaining a mean free path λ_f which is 2 orders of magnitude bigger than the size of the grain. Furthermore, the dust particles are not allowed to stick to the wall. This will reduce the amount of free floating particles in the volume and thus, reduces the amount of collisions possible. The volume should therefore be big enough to ensure a much higher probability for a particle-to-particle collision than a particle-to-wall collision. Furthermore, interactions with the wall influences the results and the statistical approach for the extrapolation of the observed results.

Secondly, the temperatures of the particles must be low enough to preserve an ice layer of the ice experiments. Furthermore, the heating of the particles at the end of these ice experiments needs to sublimate to make sure that no water drops are present in the environment. This can be enabled by maintaining a pressure in the volume ranging from 0.1 mbar to 6 mbar to stay always beneath the triple point of water in the phase diagram.

Finally, the magnetic field in the volume needs to be measured in order to detect the changes in movement when magnetic field changes. Measurements need to be done every 30 seconds. The magnetic field changes due to the influence of the Earth. These changes are of the order of minutes.

Evaluating the models described in [36], we need to observe at least 10^6 collisions to also cover unlikely collisions (e.g. colliding particles of a size $r_{eff} > 1$ mm). On the other hand it is needed that the condition $\lambda_f >> r_{eff}$ can be fulfilled. The number density of collisions per unit volume and unit time can be described by $N_{coll} = n_1 n_2 \sigma \cdot \Delta v$, where n_1 and n_2 is the number density of particles with the sizes of $r_{eff,1}$ and $r_{eff,2}$, $\sigma = \pi(r_{eff,1} + r_{eff,2})^2$ the interaction cross section (first order approximation) and Δv the relative velocity of the colliding particles. In the following sections we are going to describe how the requirements can be realised.

3. Payload

3.1. Driving requirements

In addition to the measurement requirements on the individual physical quantities specified above, requirements on the time scale and cleanliness have been set.

Table 1. The Primary Scientific Objective (PPS) is to observe the grain growth depending on variables described as a function of the Secondary Scientific Objective (SSO)

Objectives	Measurement Requirements	Reference
PSO1: Measure representative grain-size distribution of for at least 3 initial monodisperse (same size) and at least 2 polydisperse (many sizes) particle size distributions	**PMR1.1** Spatially resolve particles and grains of $r_{eff} = 0.10\,\mu$m to $10\,000.0\,\mu$m	
SSO1: Measure collision type	**SMR1.1:** Classify collision types in accordance with Güttler et. al 2010	[17]
SSO2: Measure number and sizes of collided grains as function of incident grain sizes	**SMR2.1:** Spatially resolve particles and grains as in PMR1.1. **SMR2.2:** Count the number of resulting particles	[6]
SSO3: Measure the size of collided particles as a function of initial shape type.	**SMR3.1:** Spatially resolve particles and grains as in PMR1.1. **SMR3.2:** Reconstruct the shape of the incident particles with a size bigger than $10\,\mu$m of the effective radius.	
SSO4 Measure the change in size as a function of frequency of rotation and relative angle of rotation axis of colliding grains.	**SMR4.1:** Measure the rotation frequency between 0 to 60 rot/s with an accuracy of 1%. **SMR4.2:** Measure the 3D angular velocity vector with an accuracy of 1% **SMR4.3:** Measure the 3D precession vector with an accuracy of 1% **SMR4.4:** Spatially resolve particles and grains as in PMR1.1.	
SSO5: Measure the change in size as a function of the relative incident velocity of the colliding particles.	**SMR5.1** Measure the 3D velocity vector with an accuracy of 1% **SMR5.2:** Spatially resolve particles and grains as in PMR1.1	
SSO6 Measure the change in size of the colliding particles as a function of composition of colliding grains.	**SMR6.1:** Spatially resolve particles and grains as in PMR1.1. **SMR6.2:** Composition as an input parameter.	[20]
SSO7 Measure the change in size of colliding particles as a function of initial porosity of colliding grains.	**SMR7.1:** Use monodisperse 30 micron particles with a filling factor distribution between 0.35 and 0.65. **SMR7.2:** Spatially resolve particles and grains as in PMR1.1	
SSO9 Measure the influence of ice sublimation on ice agglomerates	**SMR9.1:** Spatially resolve particles and grains as in PMR1.1 before and after temperature increase. **SMR9.2:** Measure temperature with an accuracy of 10 K, between 230 K and 300 K. **SMR9.3:** The temperature has to stay for at least 1h above 300 K	

Table 2. All experiments will be obtained with a temperature of 230 K, with a pressure of 0.1 mbar to 6 mbar with velocities ranging of $0.001\,\mathrm{ms}^{-1}$ to $5\,\mathrm{ms}^{-1}$.

Grain size distribution	Grain size [μ]	Composition	Porosity Distribution
Mono	1, 30, 50, 100	SiO_2	0.15-0.35
Mono	1, 30, 50, 100	Fayalite	0.15-0.35
Mono	1, 30, 50, 100	SiO_2 + Ice	0.15-0.35
Mono	1, 30, 50, 100	Fayalite + Ice	0.15-0.35
Mono	30	SiO_2	0.25-0.35
Mono	30	SiO_2	0.35-0.45
Mono	30	SiO_2	0.45-0.55
Mono	30	SiO_2	0.55-0.65
Poly	20-30, 0.1-100	SiO_2	0.15-0.35
Poly	20-30, 0.1-100	Fayalite	0.15-0.35
Poly	20-30, 0.1-100	SiO_2 + Ice	0.15-0.35
Poly	20-30, 0.1-100	Fayalite + Ice	0.15-0.35

The time scale of each experiment is determined by the requirement that at least 10^6 collisions must be observed, whilst maintaining a dust grain mean free path above 0.01 of the smallest dimension of the containing volume. In addition, the volume is required to be sampled for close-range measurements at least every two hours, to effectively sample the variation in the distribution of physical quantities such as size.

Due to the risk of contamination between experiments, requirements on cleanliness have been defined. No more than 20% of particles may stick to the walls of the containing volume at any time, no more than 1% of particles may remain in the chamber after each experiment, and any agitation manoeuvre used to free particles from the walls of the containing volume must not release particles with speeds above 2 mm/s in order to preserve the low velocity collision regime.

3.2. General description

Instruments are divided into two main categories: far-range instruments, which measure the particles when they are undergoing collisions in the experimental volume, and close-range instruments, which measure a subset of particles extracted from the experimental volume and brought to rest. There are three main instruments: particle tracking cameras (P-CAM), an Optical Microscope (OM), and an Atomic Force Microscope (AFM). These are used to measure the upper, middle, and lower portions of the required particle size range. Additionally, a Sample Handling and Processing (SHP) subsystem is required. Before describing the instruments in detail, we first consider the experimental volume in which dust the grains will collide.

Table 3. Specifications of the three main instruments.

	Particle tracking camera (P-CAM)	Optical Microscope (OM)	Atomic Force Microscope (AFM)
Mass (kg)	1.5	1.1	8.3
Power (W)	4	1	17
Data rate (Mbps)	5.4	0.075	0.001
Volume (mm^3)	$70 \times 70 \times 70$	$70 \times 50 \times 91$	$300 \times 250 \times 100$

The experimental volume is an aluminium cylinder with an internal volume of $6\,\mathrm{m}^3$. The volume is driven by two opposing requirements: smaller volumes increase the collision rate,
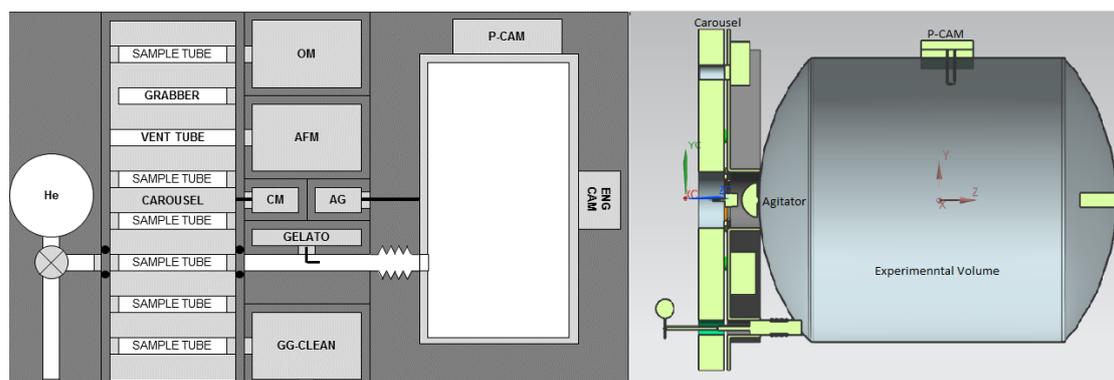
Fig. 3. The general arrangement (left): On the left the helium tank can be found. Next is the carousel containing the dust samples. Then the different instruments and the volume can be found on the right hand side. Rendering of the payload (right).

but eventually reduces the mean free path of dust grains to an unrepresentative value. $6\,m^3$ provides an optimum compromise whilst taking available launcher fairings into account. The volume is mechanically decoupled from the spacecraft structure after launch so it can be agitated for removal of particles which have adhered to the inner surface.

3.3. Far-range instruments

The experimental volume provides the attachment point for the far-range instruments. The measurement of particle positions and velocities in three dimensions requires at least two cameras (P-CAM). Since observation of collisions is a fundamental requirement, a third camera is added for redundancy and to improve precision. A $1\,cm^3$ volume will be observed at $3\,\mu m$ resolution, with the three cameras aligned orthogonally. Each camera uses focal plane arrays of 3400×3400 pixels. This will allow reconstruction of the 3D positions and velocities of all particles within the observation volume. To measure particle velocities, a frame rate of 120 frames per second is required, leading to a raw data generation rate of $13.8\,Gb\,s^{-1}$ per camera.

On-board processing of the images reduces this data volume to within the limits set by the downlink rate. The on-board processing will extract the trajectories, rotations and sizes of particles before and after collisions from the constant stream of CCD images. A single snapshot of each particle with an effective radius above $15\,\mu m$ from all three cameras will also be extracted and compressed. The onboard processing allows the total data generation rate to be reduced to below $17\,Mb\,s^{-1}$.

3.4. Close-range instruments

Since the long-range cameras can only resolve particles with sizes greater than $3\,\mu m$, additional instrumentation is required to meet the $0.1\,\mu m$ minimum particle size measurement requirement. Moreover, properties such as porosity and shape are extremely difficult to measure remotely with moving particles. Therefore, we plan to periodically extract a subset of grains from the experimental volume such that they can be presented to the OM and AFM for close-range analysis.

The OM will be used to assess the size, shape and porosity of particles in the middle of the required size range. The OM can also be used as a diagnostic tool to verify that the 'grain grabber', the device used to extract grains from the chamber, has achieved the required cleanliness level before re-insertion. Optical microscopes are common instruments and it is planned to

take advantage of flight heritage hardware from Rosetta's CIVA-M/V microscope. Therefore, the OM carries low technological risk.

Optical microscopy is diffraction limited at an object size of approximately $1\,\mu m$. Below this size, another measurement technique is required to achieve the $0.1\,\mu m$ measurement requirement.

After inspection by the OM, dust grains will be measured using the AFM to provide size and shape measurement capability down to the smallest required size of $0.1\,\mu m$ with nm precision. The measurement principle involves moving a microcantilever with a sharp tip across the dust grain, which is restrained on a substrate. Variations in the dust grain surface cause vertical deflections of the cantilever which are detected by a laser. Since the deflections are small, AFM allows for extremely high resolution, particularly in the vertical direction, down to the $10\,nm$ range.

The AFM can be operated in several modes: contact, non-contact, and 'tapping' mode. Contact mode involves moving the tip across the surface whilst maintaining a constant force on the tip. Non-contact and tapping modes involve exciting the cantilever at a resonant frequency with the tip either not contacting or contacting the surface respectively.

Atomic Force Microscopes have been used on the Phoenix lander and on Rosetta's MIDAS (Micro-Imaging Dust Analysis System) instrument. The flight heritage from these instruments means that this technology is already well-developed, and although it carries more risk due to the higher complexity compared to the other instruments, this risk is still low.

3.5. Environmental monitoring

In addition to the main instrumentation described above, the environmental conditions inside the experimental volume are required to be monitored. A range of instrumentation has been provided to record pressure, temperature, and magnetic field strength. These instruments are common, with flight heritage hardware available, and are assessed as low risk.

3.6. Sample handling and processing (SHP)

The SHP subsystem performs the functions of grain storage, injection, dispersion, sampling, and ejection, as well as maintenance of payload cleanliness. Due to its high mechanical complexity, strict cleanliness requirements, and relative novelty, the SPH subsystem is assessed as a high risk that is likely to pace the development schedule. The main part is a carousel that rotates

various components to bring them into alignment with an injection path connected to the experimental volume. These components include the individual grain canisters for each experiment, the grain grabber mechanism (described below), and a through hole to allow for chamber venting.

3.6.1. Grain grabber

The grain grabber (GG) performs the function of retrieving grains from the experimental volume and, via rotation of the carousel, presentation of grains to each close-range instrument in turn. The design comprises a collection plate to which a charge can be applied to attract and retain grains. The plate is mounted on a telescopic linear actuator which retracts back into the carousel. Once the close-range measurements have been completed, the GG is rotated into a cleaning mechanism which uses piezoelectric plate agitation, gas burst, and venting to vacuum. Although some elements of this component are common to sample handling mechanisms on other spacecraft, the requirements for this mission are unique and therefore the GG is assessed as being at TRL2. The technology development plan is outlined later in the text.

3.6.2. Ice layer generation capability (GELATO)

Due to the requirement to investigate the effects of ice layers on dust grain growth, the capability to coat grains with an ice layer is required. The current concept is to disperse water amongst dust grains which are colder than the experimental volume walls. Provided the pressure is controlled, this allows the water to condense onto the dust grains and freeze. The design is based on fuel injectors which have similar dispersal requirements but for fuel droplets to maximise combustion efficiency. High speed gas flow through static vanes generates the turbulence necessary to effectively disperse the droplets. As above, the GELATO is at TRL2.

3.7. Experiment procedure

A single experiment can be divided into three main stages: preparation, sampling, and cleaning. An experiment starts with the preparation phase. First, the carousel is rotated to align the desired grain container with the injection port. An engineering camera, located at the top of the experimental volume, is started. High-pressure helium is then used to drive the dust grains into the experimental volume, and if an ice layer is required, water is dispersed. The injector generates turbulence which effectively breaks up any agglomerates that may have formed in storage. Particle tracking cameras record the collisions. To prevent excessive particle build-up on the walls, the chamber is periodically agitated using an off-axis motor and low-amplitude resonator.

At set intervals, close-range measurements are required. First, the carousel will align the GG with the injection port. The GG collection plate is then extended into the experimental volume to collect a sample, before retracting back into the carousel. The carousel rotates to align the GG with the OM and AFM in turn for close-range measurements. Once all close-range measurements are completed, the carousel rotates again to present the GG to a cleaning area. This process can be repeated as required, with OM inspections to ensure GG cleanliness.

Once the experiment finishes, the experimental volume must be cleaned. First, the carousel is rotated to allow high-pressure helium to pressurise the experimental volume. Second, the experimental volume is agitated. Third, the volume is vented to space with the flow modulated to entrain particles. This process can be repeated as required to clean the chamber. Once all valves are closed the experiment is complete.

3.8. Technology development

Due to the novelty of the mission objective and relative immaturity of some instruments, in particular the grain grabber and the GELATO which are currently at Technology Readiness Level (TRL) 2, a technology development programme is required. Verification of individual components of the sample handling and processing subsystem will first be performed in the laboratory, before integrated sub-system testing in microgravity, for example on parabolic flights. Despite the above, the measurements remain feasible in principle.

4. Mission Design

Considering the scientific objectives and requirements presented in Sec. 2, the two main mission objectives are to conduct all the planned science experiments and to retrieve the data products generated by the payload (see Sec. 3). Hence, we highlight five main requirements for the mission. The need to provide a continuous micro-gravity environment is a necessary criterion for conducting the experiments, as is the need to protect the experiments from major external disturbances. To avoid contamination between experiments conducted in the chamber, a decontamination time and process must be taken into account. The experiment chamber walls must be highly thermally controlled so that the pressure and temperature remain homogeneous over the whole volume. The high resolution cameras within the payload will generate a large amount of processed data. Consequently the service module must provide the downlink rate needed to effectively transfer this data to Earth.

4.1. Mission Timeline

The nominal mission orbital lifetime is 5 years, with a goal of 10 years. Before the experimental mission begins, the performance of the bus and payload must be assessed. Table 4 presents the concept of operations.

4.2. Launcher & Orbit

The satellite will be sent into orbit by a Soyuz launch vehicle departing from the Guyana Space Center. The high reliability and the precision of this Russian launcher are a main driver for this choice. A 3σ accuracy leads to an uncertainty of $\pm 12\,\mathrm{km}$ for the altitude and $\pm 0.12°$ for the inclination. To mitigate the risk of having any debree on the final orbit an injection orbit of $785\,\mathrm{km}$ is chosen. After the successful injection, an orbit correction manoeuvre to reach the final nominal SSO orbit of $800\,\mathrm{km}$ of altitude and an inclination of $98.6°$ and the RAAN of 6AM/6PM. is performed. The main advantages of the chosen SSO are:

– Long access times for the Downlink
– Thermal stability due to a constant sun angle
– No attitude manoeuvres to point the sun
– Low Drag & Solar pressure acceleration $10^{-7}\mathrm{ms}^{-2}$

When the EOL is reached, a de-orbiting manoeuvre is planned. Since the mass of the spacecraft is above the critical limit of $1000\,\mathrm{kg}$ future analyses have to be made to ensure the

Table 4. Concept of operation of Magrathea satellite.

Phase	Details	Length
Pre-flight	Assembly test and launch operations	9 months
Transit	Mount spacecraft on launcher Control environment conditions on launch	2 months
Launch	Soyuz launcher Sun-Synchronous (800 km) Shared ride if possible (mass < 2 t)	1 day
Detumble	Stabilize Obtain attitude	1 day
Commissioning	Deploy communication and solar System check Initiate science	30 days
Experiment	Release sample Take continuous measurements Take close-up measurements Vent chamber	5 years
End of lifetime	Thrusters firing Final perigee (520 km)	25 years

safe disposal of the satellite. For our purpose, a standard disposal time of 25 years is taken into account and calculated. The perigee is lowered to 520 km of height by the de orbit manoeuvre in order to exploit the aerodynamic brake to dispose the spacecraft in the mentioned time. The overall Δv budget for the single manoeuvre is shown in Table 5

Table 5. Analysis of Δv budget for different manoeuvres. Station keeping is taken for 10 years, as an example.

Manoeuvre	Delta V [m/s]	Fuel mass [kg]
Injection	37.85	15.3
Station Keeping - Inclination	51	17
Station Keeping - Drag	24	8
Collision avoidance	1	0.3
Deorbit	74.8	31.1
Total	188.7	71.7

4.3. Environment

On a low orbit the drag becomes more important, while at a higher altitude the radiation intensity due to crossing the Van Allen Belts increases. AN 800 km orbit was chosen because at this attitude the solar radiation pressure and the drag forces reach the same order of magnitude: the resulting acceleration on the satellite is 10^{-7}ms^{-2}. To monitor the effect of the Earth's magnetic field the payload will include a magnetic field measurement system.

5. Spacecraft

5.1. Structure & Mechanisms

The driving requirements for the spacecraft structure are as follows:

- Size and shape sized for the Soyuz launch vehicle
- Structure capable of withstanding launch loads
- Accommodate the experiment chamber of 6 m^3 in volume and experiment instruments

- Accommodate the deployable solar panels and Sun shield
- Accommodate 3-axis stabilisation

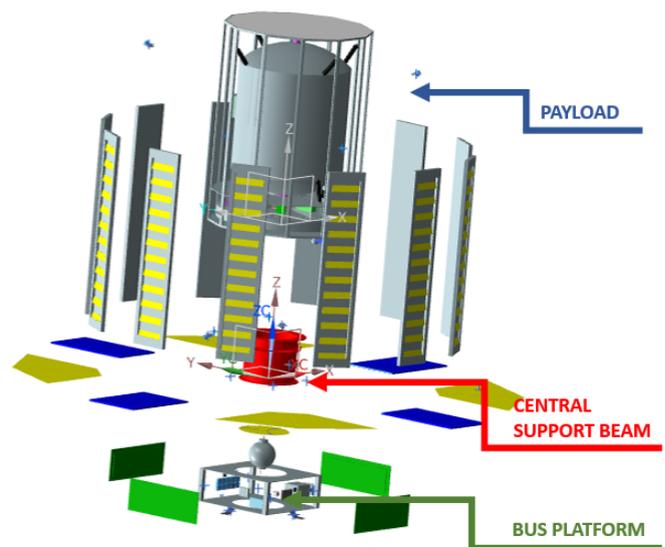The following configuration was chosen:

The instrument bus is in a box configuration, with wall panels mounted to a frame for easy access to the electronics. Instrument distribution was optimised in such a way that the bus COM aligns with the spacecraft axis. The launch loads are carried by a central load-carrying beam.

The solar panels and the Sun shield are mounted to the bottom of the frame with the use of industry standard solar array drive mechanism.

The payload, comprising the experiment chamber and instrument shelves, is mounted inside the dodecagonal frame. The frame is connected to the aforementioned load-carrying beam via a flange interface.

The instrument chamber is mounted on springs to enable chamber agitation as for the experiment requirements. The instrument shelves are connected directly to the frame.

The material for the primary structures of the spacecraft is aluminium and CFRP honeycomb core panels are used for secondary structures with low loads. The project does not have specific requirements to control for thermal expansion, such is the case with optical payloads.

Fig. 4. Exploded view of the spacecraft, showing the tank on the top, louvres on the sides and the bus at the bottom

5.2. Thermal Control

The orbit altitude is fixed to 800 km, therefore the main heating fluxes are Sun's radiation, reflected Sun radiation from the Earth and IR radiation from the Earth.

To maintain an operating temperature of the payload structure below 230 K, it is necessary to cover it with louvre doors, with aluminium coating. Louvres that are facing the Earth are closed and reflect the IR radiation. Louvres that are facing deep space are opened. The payload structure underneath the louvres is painted black to maximise heat outflow to deep space. To minimise radiation from the louvres to the inside structure, the inside of the louvres is coated with vaporised deposited gold.

The bus and the payload structure are detached and held together by a low conducting structure to avoid heat exchange. To eliminate temperature variations of the experiment chamber due to heat gradients, the chamber has to be made of highly conductive material. The surface of the payload structure facing the bus is therefore covered with Multi Layer Insolation (MLI). Because the back of the spacecraft is sometimes facing the earth it is coated with a quartz mirror.

Table 6. Results obtained from steady state model for the payload and spacecraft bus structure.

		Temperature [K]	
		Cold	Hot
Payload	With louvres	~161	~190
Spacecraft	With heaters	~263	~293

We used a steady state model to calculate the equilibrium temperatures for the payload structure both for Sun illumination and eclipse. The results are shown in Tab. 6 and they are below the upper limit of 230 K when louvres are used.
The expected operating temperature of the electronics and the batteries within the bus is -10°C to 50°C. The bus structure is covered with MLI.

We also used a steady state model was to estimate the equilibrium temperature of the bus structure and the results are shown in Tab. 6. To heat the payload structure to 300 K, all the louvres facing the sun are opened and the louvres facing deep space are closed. To measure the temperatures of the subsystems, thermocouples are used.

A more detailed thermal analysis will be performed at later stages to improve understanding of the thermal regimes, especially the internal heat fluxes of the payload.

5.3. Attitude and Orbit Control

The main driver for the Attitude and Orbit Control (AOCS) subsystem is minimising accelerations imparted to particles by the walls of the experimental chamber. When translating it to a subsystem requirement, it means that we have to detect an acceleration higher than 8×10^{-10} ms^{-2}, whilst the experiments are being conducted. Due to the spacecraft high frontal surface area with the sun shield and solar panels, the solar radiation pressure will create an acceleration of the order 10^{-7} ms^{-2}. An order of magnitude lower we have the albedo radiation, and another one the drag. These are applied on the side surface of the spacecraft. To summarise, the resulting force for our spacecraft is about 200 µN. With accelerations three orders of magnitude higher than the requirement, we devised a system capable of detecting and counteracting the accelerations. Therefore, the most important components of the system is a drag free accelerometer and field-emission electric propulsion (FEEP) thrusters. The accelerometer comes from the flight heritage of BepiColombo, LISA pathfinder and GOCE missions, with higher accuracies than the one required [21], while the FEEP is an AMR nano thruster capable of 10 µN up to 0.5 mN [3]. For the rest of the spacecraft operations, i.e. no experiments are being conducted, the AOCS is composed of standard components, as there are not stringent requirements in pointing. To sense the attitude we use four sun sensors (with ≤ 0.1° rms accuracy), two star trackers (with 5 arcsec cross-boresight), an inertial measurement unit (with 300 µg and 1 °/hour acceleration and rotation accuracies,

respectively) [27, 29, 31]. The orbit is determined using a Surrey GPS with an error of 10 m in position and 0.15 ms^{-1} in velocity [32]. For attitude control the spacecraft has control momentum wheels capable of generating a torque of 45 Nm and magnetotorquers generating a maximum dipole momentum of 100 Am^2 [2, 28].

5.4. Power

For LEO and SSO orbits the most efficient power supply are the solar arrays. The power supply chain is composed of the solar arrays, the power distribution control unit (PDCU) and the batteries. To allow a proper and safe sizing of the arrays an efficiency of 0.2 is assumed as well as a degradation factor of 0.8 for the EOL. As a result, a total surface of 6.3 m^2 has to be provided. We select GaInP2/GaAs/Ge, which have significant flight heritage. The generated power is handled by the PDCU which is able to handle a peak power of 900 W. Triple redundancy is provided from the component itself. For this task, the board from company ASP is chosen. Twice a year a peak shadow phase of 18 minutes is reached, which is compensated by the battery. The battery subsystem is designed to allow depth of discharge (DOD) of 55%. The remaining capacity at the end of life after 10 years, planned to be 80%. Therefore, a total required storage capacity is 1000 W/h. This budget is fulfilled by using 10 Li-ion cells of type EaglePicher SLC-028-01.

5.5. Communications

The communication system is driven by the payload data rate requirements. Table 7 shows link budgets for Telemetry, Tracking & Commanding (TT&C) and payload data downlink along with the requirements that guarantee communication. TT&C has a low data volume, but it is crucial for housekeeping maintenance. Two S-band patch antennas will be mounted pointing in different directions, with one transceiver per antenna [15, 16]. A relatively small bandwidth of 100 kb/s for the uplink and 2 Mb/s for the downlink is sufficient to provide a good energy per bit to noise power spectral density ratio (EB/N0) even when the signal is weak. Using a modulation scheme such as QPSK with Reed-Solomon FEC (Forward Error Correction), we can be confident enough that we will have a bit error rate of at most 10^{-4}. A specific system for payload data downlink is necessary, as the instruments can generate around 190 GB/day. One X-band horn antenna is used [1] which allows a data rate of up to 175 Mbps. Assuming 12 passes per day, this rate allows all data to be downloaded the same day. A modulation scheme, such as 8-PSK with Reed-Solomon FEC, is needed. This requires an EB/N0 ratio of 14 dB in order to have a bit error rate of 10^{-6}.

Table 7. Link budget for TT&C (S-Band) and data downlink (X-Band).

	S up (100 kbps)	S down (2 Mbps)	X down (175 Mbps)
EIRP [dBW]	32.2	-2	17.8
Path losses [dB]	157	157.4	169.1
G/T [dB/K]	-22	9.6	37.3
EB/N0 [dB]	30	13.9	30.1
Required EB/N0 [dB]	8	8	14
Margin [dB]	22	5.9	16.1

5.6. Onboard Computer & Data Handling

The high data volume and need for on-board image processing drives the spacecraft computer selection. Two On-Board Computer Data Handling (OBDH) systems are used.

The first OBDH subsystem is linked to the payload. Its main purpose is to process data from the cameras and store a subset in memory (less than 16 GB per day). The second OBDH subsystem has the task of acquiring, formatting and encoding spacecraft telemetry and downlinking data to the ground stations.

A *Sirius C&DH* computer has been chosen for the payload. It has a 32-bit OpenRISC fault-tolerant processor with a mass memory storage of 16 GB. The power supply is 16 V. This unit shall be operating raw data compression as well as some simple data analysis.

OBDH VPDHS has been chosen for the S/C operations. Its storage capacity is 4 GBytes and the power consumption is 15 W.

5.7. Propulsion

The propulsion subsystem has to carry out the following functions:

- Orbit injection and correction manoeuvre
- Detumbling phase
- Station keeping (inclination for a lifecycle of 10 years)
- Collision avoidance
- De-orbiting[1]

Considering the Δv budget (shown in Table 5), we performed a trade-off analysis in order to choose the correct kind of thrusters and their number. From this analysis we have selected a Monopropellant Hydrazine Thruster. Furthermore, the choice was also driven by the mission's lifetime (between 5 and 10 years). Four thrusters will be installed to ensure a symmetry configuration without changing the centre of gravity, each with a thrust of 24.6 N and I_{sp}=230 s. Through the Tsiolkovsky equation, we calculated the mass of the fuel needed for all manoeuvres, resulting in M_{fuel}=75 kg. From that the volume of the tank needed is V_{tank}=8.5 kg. Drag perturbations will be compensated by utilization of electrical propulsion (FEEP thrusters), which are a part of the AOCS budget.

5.8. Mass & Power Budget

Table 8. Breakthrough of mass and power budgets for the spacecraft. Mass is shown with margin, specified in parenthesis.

Subsystem	Mass [kg]	Power [W]
Payload (+35%)	289	454
Telecom (+20%)	22.7	66
OBDH (+20%)	2,8	18
Power (+20)	29	27
AOCS (+20%)	84	266
Propulsion (+20%)	37	24
Thermal (+20%)	121	36
Structure (+20%)	373	0
Propellant (+20%)	75	0
Total	**1033**	**891**

---

[1] Considering the weight of our spacecraft (medium satellite), we took into account to carry out the burn-up/break-up (BUBU) manoeuvre for the disposal phase

Table 8 shows over all mass and power budget for the mission. We note that an existing satellite bus can be reused, such as Airbus Astrosat-1000 bus, which can accommodate satellites with total mass between 800 and 1200km. This bus was used for constellation of remote sensing satellites Pleiades. The attitude control requirements on our mission can be relaxed, compared to Pleiades.

6. Ground Segment

For an almost polar orbiting satellite, a single high latitude ground station can provide good coverage. That is why the KIR-1 15 m antenna at Kiruna Estrack ground station in northern Sweden will be used for the data downlink. With this antenna, and the satellite at a sun synchronous orbit at 800 km, we will have 12 access windows per day, with a mean duration of 730 s per window. For housekeeping operations, the REDU-3 2.4 m antenna at Redu ground station will be the most adequate, because there is a low volume of data to be transferred.

7. Programmatic

7.1. Preliminary cost analysis

As a first approximation, we estimate that the satellite will fall within an M-class Cosmic Vision budget. The preliminary cost analysis is presented in Table 9. The payload costs are charged to the national agencies and laboratories from the scientific consortium. Conversely, the spacecraft, operations and mission management will be financed by the Alpbach Space Agency (ASA). Risk analysis is shown on Figure 5.

Table 9. Preliminary cost analysis.

Spacecraft Elements	Cost (M€)
Payload	88
Spacecraft bus	135
Mission and Programmatic Elements	
Satellite (total)	223
ESA program level	27
Integration, assembly and test	22
Ground operations	31
Flight software	20
Launch vehicle	75
Total (10% margin)	**438**

7.2. Risk Assessment

A risk analysis has been performed and nine risks were identified. These are shown in Fig. 5, with each risk ranked with a probability and severity mark.

8. Conclusion

Magrathea will be a mission to investigate the physics behind one of the biggest problems in astrophysics: how the planets form from dust in protoplanetary disks. The goal of our mission is to observe the physics and conditions that allow grains to grow from the microscopic scale to the macroscopic scale. We propose to execute a set of 28 experiments in microgravity on board an orbiting spacecraft. A set of instruments, including optical microscope, tracking cameras and an atomic force microscope will
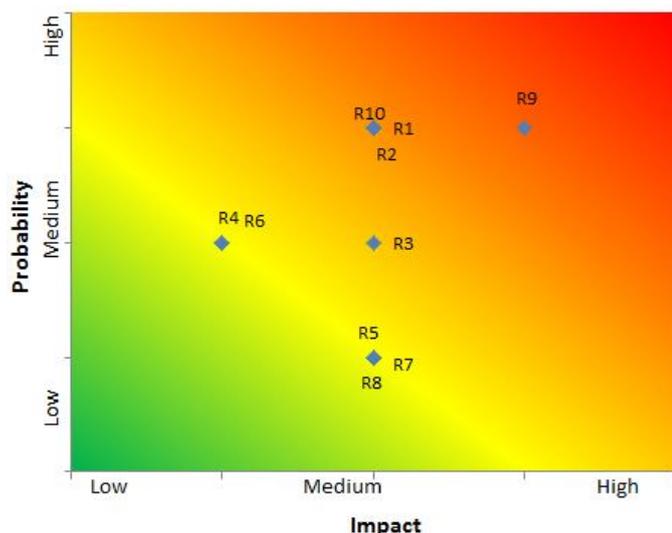
Fig. 5. Risk analysis the mission using NASA risk matrix. Risks R9 (sample handling system), R10 (particles sticking to the wall), R1 (chamber agitation), R2 (chamber contamination) are the most critical to the development of this mission and additional testing is foreseen.

allow us to monitor growth of the particles and investigate their shape. The spacecraft will fly in an 800 km sun synchronous orbit. The spacecraft bus can probably be derived from one of the existing industry buses (e.g. Astrosat-1000) providing a significant cost saving. The space laboratory will be in orbit around Earth for 5 to 10 years and provide the science community with unique information about grain interactions in a simulated protoplanetary disk like environment.

References

[1] A-Info (2016). Fact Sheet - LB-90-10 Standard Gain Horn Antenna.
[2] Airbus Defense & Space (2016). Fact Sheet - CMG 15-45S.
[3] AMR Propulsion Technologies (2017). Fact Sheet - Introduction to the IFM Nano Thruster.
[4] Blum, J., Beitz, E., Bukhari, M., Gundlach, B., Hagemann, J.-H., Heißelmann, D., Kothe, S., Schräpler, R., von Borstel, I., and Weidling, R. (2014). Laboratory Drop Towers for the Experimental Simulation of Dust-aggregate Collisions in the Early Solar System. *Journal of Visualized Experiments*, (88).
[5] Blum, J. and Wurm, G. (2001). Drop tower experiments on sticking, restructuring, and fragmentation of preplanetary dust aggregates. *Microgravity Science and Technology*, 13(1):29–34.
[6] Blum, J. and Wurm, G. (2008a). The growth mechanisms of macroscopic bodies in protoplanetary disks. *Annu. Rev. Astron. Astrophys.*, 46:21–56.
[7] Blum, J. and Wurm, G. (2008b). The Growth Mechanisms of Macroscopic Bodies in Protoplanetary Disks. *Annual Review of Astronomy and Astrophysics*, 46(1):21–56.
[8] Blum, J., Wurm, G., Kempf, S., and Henning, T. (1996). The brownian motion of dust particles in the solar nebula: an experimental approach to the problem of pre-planetary dust aggregation. *Icarus*, 124(2):441–451.
[9] Borucki, W., Koch, D., Basri, G., Batalha, N., Brown, T., Caldwell, D., Caldwell, J., Christensen-Dalsgaard, J., et al. (2010). Kepler planet-detection mission: Introduction and first results. *Science*, 327(5968):977–980. cited By 1012.
[10] Brisset, J., Colwell, J., Dove, A., Maukonen, D., Brown, N., Lai, K., and Hoover, B. (2015a). Nanorocks: Studying planet formation and planetary rings on the international space station. In *European Planetary Science Congress 2015, held 27 September-2 October, 2015 in Nantes, France, Online at http://meetingorganizer. copernicus. org/EPSC2015, id. EPSC2015-767*, volume 10.
[11] Brisset, J., Colwell, J., Dove, A., Maukonen, D., Brown, N., Lai, K., and Hoover, B. (2015b). NanoRocks: Studying Planet Formation and Planetary Rings on the International Space Station. In *European Planetary Science Congress 2015*, volume 10, pages EPSC2015–767, Nantes, France.

[12] Brisset, J., Heißelmann, D., Kothe, S., Weidling, R., and Blum, J. (2013). The suborbital particle aggregation and collision experiment (space): Studying the collision behavior of submillimeter-sized dust aggregates on the suborbital rocket flight rexus 12. *Review of Scientific Instruments*, 84(9):094501.
[13] Broeg, C., Fortier, A., Ehrenreich, D., Alibert, Y., Baumjohann, W., Benz, W., Deleuil, M., Gillon, M., Ivanov, A., Liseau, R., Meyer, M., Oloffson, G., Pagano, I., Piotto, G., Pollacco, D., Queloz, D., Ragazzoni, R., Renotte, E., Steller, M., and Thomas, N. (2013). Cheops: A transit photometry mission for esa's small mission programme. *EPJ Web of Conferences*, 47. cited By 53.
[14] Dominik, C. and Tielens, A. (1997). The physics of dust coagulation and the structure of dust aggregates in space. *The Astrophysical Journal*, 480(2):647.
[15] Elta (2016). Fact Sheet - S-Band Transceiver.
[16] EnduroSat (2016). User Manual - S-Band Patch Antenna Type I.
[17] Güttler, C., Blum, J., Zsom, A., Ormel, C. W., and Dullemond, C. P. (2010). The outcome of protoplanetary dust growth: pebbles, boulders, or planetesimals?-i. mapping the zoo of laboratory collision experiments. *Astronomy & Astrophysics*, 513:A56.
[18] Güttler, C., Blum, J., Zsom, A., Ormel, C. W., and Dullemond, C. P. (2010). The outcome of protoplanetary dust growth: pebbles, boulders, or planetesimals? *Astronomy and Astrophysics*, 513:A56.
[19] Haynes, W. M. (2012). *CRC Handbook of Chemistry and Physics*. CRC Press, 93rd edition edition.
[20] Heißelmann, D., Fraser, H. J., and Blum, J. (2011). Experimental studies on the aggregation properties of ice and dust in planet-forming regions. *arXiv preprint arXiv:1106.4760*.
[21] Iafolla, V., Fiorenza, E., Lefevre, C., Morbidini, A., Nozzoli, S., Peron, R., Persichini, M., Reale, A., and Santoli, F. (2010). Italian Spring Accelerometer (ISA): A fundamental support to BepiColombo Radio Science Experiments. *Planetary and Space Science*, 58(1-2):300–308.
[22] Keller, L., Hony, S., Bradley, J., Molster, F., Waters, L., Bouwman, J., De Koter, A., Brownlee, D., Flynn, G., Henning, T., et al. (2002). Identification of iron sulphide grains in protoplanetary disks. *Nature*, 417(6885):148–150.
[23] Knutson, H. (2007). Extrasolar planets: Water on distant worlds. *Nature*, 448(7150):143–145. cited By 11.
[24] Love, S. G., Pettit, D. R., and Messenger, S. R. (2014). Particle aggregation in microgravity: Informal experiments on the international space station. *Meteoritics & Planetary Science*, 49(5):732–739.
[25] NASA (2017a). Cosmic dust aggregation experiment.
[26] NASA (2017b). The Zero Gravity Research Facility.
[27] NewSpace Systems (2016a). Fact Sheet - Fine (Digital) Sun Sensor.
[28] NewSpace Systems (2016b). Fact Sheet - Magnetorquer Rod.
[29] Northrop Grumman (2017). Fact Sheet - LN-200S Inertial Measurement Unit.
[30] Pollack, J. B., McKay, C. P., and Christofferson, B. M. (1985). A calculation of the rosseland mean opacity of dust grains in primordial solar system nebulae. *Icarus*, 64(3):471–492.
[31] Sinclair Interplanetary (2016). Fact Sheet - Second Generation Star Tracker (ST-16RT2).
[32] Surrey Satellite Technology (2016). Fact Sheet - SGR-20.
[33] Testi, L., Birnstiel, T., Ricci, L., Andrews, S., Blum, J., Carpenter, J., Dominik, C., Isella, A., Natta, A., Williams, J. P., and Wilner, D. J. (2014). Dust Evolution in Protoplanetary Disks. In *Protostars and Planets VI*. University of Arizona Press.
[34] Wada, K., Tanaka, H., Suyama, T., Kimura, H., and Yamamoto, T. (2007). Numerical simulation of dust aggregate collisions. i. compression and disruption of two-dimensional aggregates. *The Astrophysical Journal*, 661(1):320.
[35] Wada, K., Tanaka, H., Suyama, T., Kimura, H., and Yamamoto, T. (2008). Numerical simulation of dust aggregate collisions. ii. compression and disruption of three-dimensional aggregates in head-on collisions. *The Astrophysical Journal*, 677(2):1296.
[36] Zsom, A., Ormel, C. W., Güttler, C., Blum, J., and Dullemond, C. P. (2010). The outcome of protoplanetary dust growth: pebbles, boulders, or planetesimals? II. Introducing the bouncing barrier. *A&A*, 513:A57.

Europe and Australia